ChemistrySelect

Research Article
doi.org/10.1002/slct.202301789

Chemistry Europe
European Chemical Societies Publishing

www.chemistryselect.org

A $CoFe_2$ Alloy-Functionalized Few-Layer Graphene Sheet Nanocomposite as an Electrocatalyst of the Oxygen Reduction Reaction

Xiqiong Guo,[a] Fangying Yuan,[a] Peixi Wang,[a] Runqiu Li,[a] and Hui Zheng*[a]

Searching for a high-efficiency, recycled and cheap catalytic material for oxygen reduction reaction (ORR) is urgently needed in fuel cells. In this study, we successfully fabricated a nanocomposite consisting of $CoFe_2$ alloy functionalized few-layer graphene sheets ($CoFe_2$/FLGs) by employing ferric nitrate, cobalt nitrate, and glucose as precursors. Various measurements conducted in this research confirm that the nanosized $CoFe_2$ alloy particles are evenly dispersed within the FLGs and possess significant magnetism. Electrochemical measurements reveal that the $CoFe_2$/FLGs exhibit a high positive onset potential (0.901 V), follow a four-electron pathway, display a low Tafel slope (77.21 mV/dec), possess a low charge-transfer resistance (~72 Ω), and exhibit strong methanol tolerance. Consequently, the resulting $CoFe_2$/FLGs nanocomposite demonstrates excellent electrocatalytic performance and recyclability for the ORR, positioning it as a promising catalyst for fuel cells.

Introduction

In recent years, fuel cells have garnered significant attention, both domestically and internationally, as efficient and clean electrochemical power generation devices, owing to the growing importance of environmental issues and energy challenges.[1–3] The oxygen reduction reaction (ORR)[4–6] is a crucial factor that directly influences the energy conversion efficiency of fuel cells. However, the ORR process involves multiple electron transfer steps and sluggish reaction kinetics, which have become a bottleneck impeding the advancement of fuel cells.[7–10]

Presently, Pt-based precious metals remain the most effective catalysts for ORR. Nonetheless, their utilization in large-scale commercial electrocatalytic reactions is impractical due to their low abundance in the Earth's crust, high cost, and inherent instability.[11–13] Therefore, the development of non-precious catalytic materials for ORR that are low-cost, recyclable, highly active, and stable holds significant importance in promoting the widespread commercial application of fuel cells.[14–17] Graphene, owing to its unique electrical characteristics and superior oxygen reduction activity compared to other catalysts, has gained considerable attention as a catalyst support.[18–20] To enhance the performance of single-component graphene materials, which possess few active sites and weak electrochemical activity, the internal structure of graphene is commonly modified by introducing heteroatoms or metal oxides.[21–25] J. Wang et al.[24] employed ammonium ferric citrate as a precursor to prepare Fe/Fe_3C nanoparticles encapsulated in N-doped carbon through acid leaching after pyrolysis in an argon atmosphere, and demonstrated its excellent ORR catalytic activity. S. Guo et al.[26] discovered that the synergistic effect of metal Co nanoparticles, nanoscale CoO catalysts, and graphene supports effectively enhanced the ORR performance of the catalyst materials. Q. Feng et al.[27] fabricated a γ-Fe_2O_3/reduced Graphene oxide (rGO) nanocomposite and demonstrated its high ORR catalytic activity and recyclability due to the presence of Fe_2O_3 magnetic particles. However, the limited magnetism or weak binding of these metal or oxide particles with graphene restricts their recyclability and hampers their ORR performance.

In this study, we successfully fabricated a non-precious, highly efficient, and recyclable $CoFe_2$ alloy/FLGs nanocomposite by utilizing ferric nitrate, cobalt nitrate, and glucose as precursors. The $CoFe_2$ alloy particles with nanoscale size exhibit uniform dispersion on the graphene surface, facilitated by strong binding forces. This not only promotes efficient electron transfer between $CoFe_2$ and graphene but also enhances the recyclability of the catalyst. Detailed investigations were conducted on the crystal structure, microstructure, and morphology of the synthesized $CoFe_2$ alloy/FLGs nanocomposite. Furthermore, the ORR performance and stability of the nanocomposite were thoroughly examined. The results demonstrate that the synthesized $CoFe_2$ alloy/FLGs nanocomposite exhibits excellent electrocatalytic activity for ORR.

Materials and Methods

Preparation of the $CoFe_2$ alloy/FLGs Nanocomposite

To begin, a sol-gel method was employed to synthesize nanoscale cobalt ferrite. Raw materials including cobalt nitrate and ferric nitrate nonahydrate were utilized with a molar ratio of 1:2. Ferric nitrate and cobalt nitrate were of analytical pure grade and purchased from Aladdin Chemical Reagent Corpo-

[a] X. Guo, F. Yuan, P. Wang, R. Li, Prof. H. Zheng
Department of Electronics Science and Technology, Hangzhou Dianzi University
Laboratory for Nanoelectronics and NanoDevices
Hangzhou Dianzi University, Hangzhou 310018, China.
E-mail: zhenghui0551@hdu.edu.cn

ration. Citric acid monohydrate (99.5%) was weighed at twice the molar ratio of the metal ions, and the materials were mixed and dissolved. Ammonia was then added dropwise until the solution reached a neutral pH. The mixture was heated in a water bath at 80 °C until it formed a gel-like substance, dried, and subsequently placed in a muffle furnace at 900 °C for 3 h to obtain nanoscale cobalt ferrite.

Next, the obtained cobalt ferrite was mixed with glucose (99.7%) in a molar ratio of 1:10, dissolved in deionized water, and heated to 150 °C. When the mixed solution reached a viscous consistency, it was dropwise spin-coated onto a spin-coater and dried under a baking lamp for 12 h. The resulting mixture was then placed in a vacuum tube furnace, pumped to a pressure of 5×10^{-4} Pa, and held at 1100 °C for 2 h. The amount of the $CoFe_2$ alloy in the composite is estimated to 20 wt%.

Characterization Technique

The morphology of the $CoFe_2$ alloy/FLGs was examined using a field emission scanning electron microscope (FESEM, JEOL 7800F) and a transmission electron microscope (TEM, JEOL-JEM 2100). The crystallinity of the $CoFe_2$ alloy particles and FLGs was analyzed using X-ray diffraction (XRD, Rigaku IV) and Raman scattering spectra (Horiba Evo Nano with a 532 nm laser), respectively. The chemical composition and bonding state of the catalyst were determined using X-ray photoelectron spectroscopy (XPS, Thermo Avantage ESCALAB 250Xi) and an Energy Dispersive Spectrometer (EDS). The magnetic properties were measured using a vibrating sample magnetometer (VSM).

Electrochemical Behavior Study

The electrocatalytic performance of the $CoFe_2$ alloy/FLGs nanocomposite was evaluated using cyclic voltammetry (CV), linear sweep voltammetry (LSV) with a rotating disk electrode (RDE) and a rotating ring disk electrode (RRDE) (CHI instrument 760E, USA). A glassy carbon electrode (GCE) modified with the $CoFe_2$ alloy/FLGs catalyst, a carbon rod, and a Hg/HgO electrode were used as the working, counter, and reference electrodes, respectively. The $CoFe_2$ alloy/FLGs catalyst ink was prepared by dispersing 8 mg of the $CoFe_2$ alloy/FLGs in 1500 μL of ethanol solvent, adding 100 μL of Nafion solution, and sonicated for 1 h. Then, 5.8 μL of the catalyst ink was pipetted onto the electrode surface and allowed to dry naturally at 25 °C. The catalyst loading on the electrode surface was estimated to be 0.41 mg/cm^2.

Before conducting electrochemical measurements, a 0.1 mol/L KOH solution was purged with N2 for 30 minutes. CV tests were performed using the three-electrode system mentioned earlier in a N_2 or O_2 saturated 0.1 mol/L KOH solution. The potential window ranged from −1.2 to +0.2 V versus Hg/HgO, and the scan rate was set at 10 mV s^{-1}. Throughout the measurements, a continuous flow of oxygen was maintained over the 0.1 mol/L KOH solution to ensure oxygen saturation. LSV measurements were carried out at speeds ranging from 250 to 3000 rpm and potentials ranging from +0.2 to −1.2 V versus Hg/HgO. Besides, the hydrogen peroxide yield (H_2O_2%) and the electron transfer number (n) were given by RRDE. The electrochemical impedance spectroscopy (EIS) was measured in the frequency range from 1 MHz-10 mHz with a voltage amplitude of 5 mV. The electro-catalysts stability of the $CoFe_2$ alloy/FLGs nanocomposite was evaluated at a voltage sweep rate of 10 mV/s in oxygen saturated 0.1 mol/L KOH solution for 1000 cycles. During the response process, a methanol poisoning resistance test was conducted by adding 2 mL of 0.5 mol/L methanol at 1000 s.

Results and Discussion

Firstly, the morphology and microstructure of the $CoFe_2$ alloy/FLGs nanocomposite were characterized using FESEM and TEM, as depicted in Figure 1. Figure 1a displays a low-magnification FESEM image, revealing a well-developed lamellar graphene structure with high crystallinity and a few-layer configuration, evident from its transparent appearance.[28] Furthermore, the high-magnification FESEM image in Figure 1b illustrates the uniform embedding of $CoFe_2$ alloy particles within the FLGs. The TEM image in Figure 1c further confirms the uniform distribution of nanoscale $CoFe_2$ particles on the lamellar graphene sheets. The insert in Figure 1c demonstrates a Gaussian distribution of $CoFe_2$ particle sizes, with an average diameter of 20.8 nm. HRTEM analysis captured representative $CoFe_2$ particles coated with FLGs, as shown in Figure 1d. The linear contours of the selected areas (S1 and S2) are also presented in Figure 1e. The lattice spacing of S1 measures

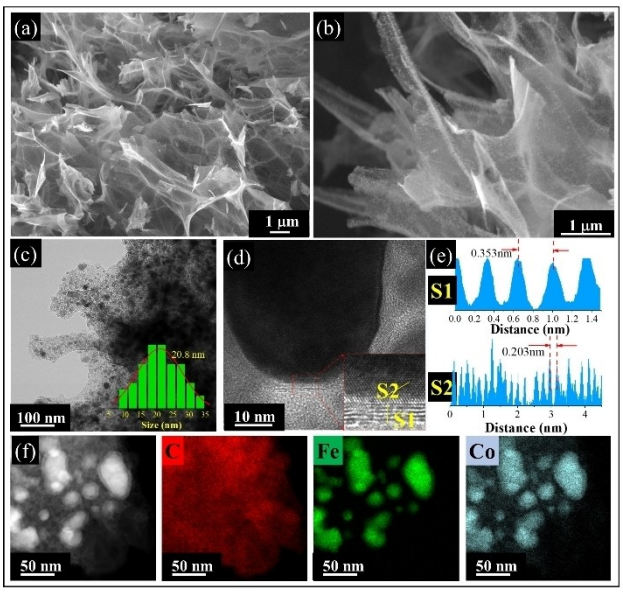

Figure 1. The morphology and microstructure of the $CoFe_2$ alloy/FLGs nanocomposite. (a) FESEM image at ×7000; (b) FESEM image at ×19000; (c) TEM image, the inset is the size distribution of $CoFe_2$ particles; (d) HRTEM image, the inset is the selected area magnification. (e) The line profile of the S1 and S2; (f) Elements mapping of the corresponding C, Fe and Co.

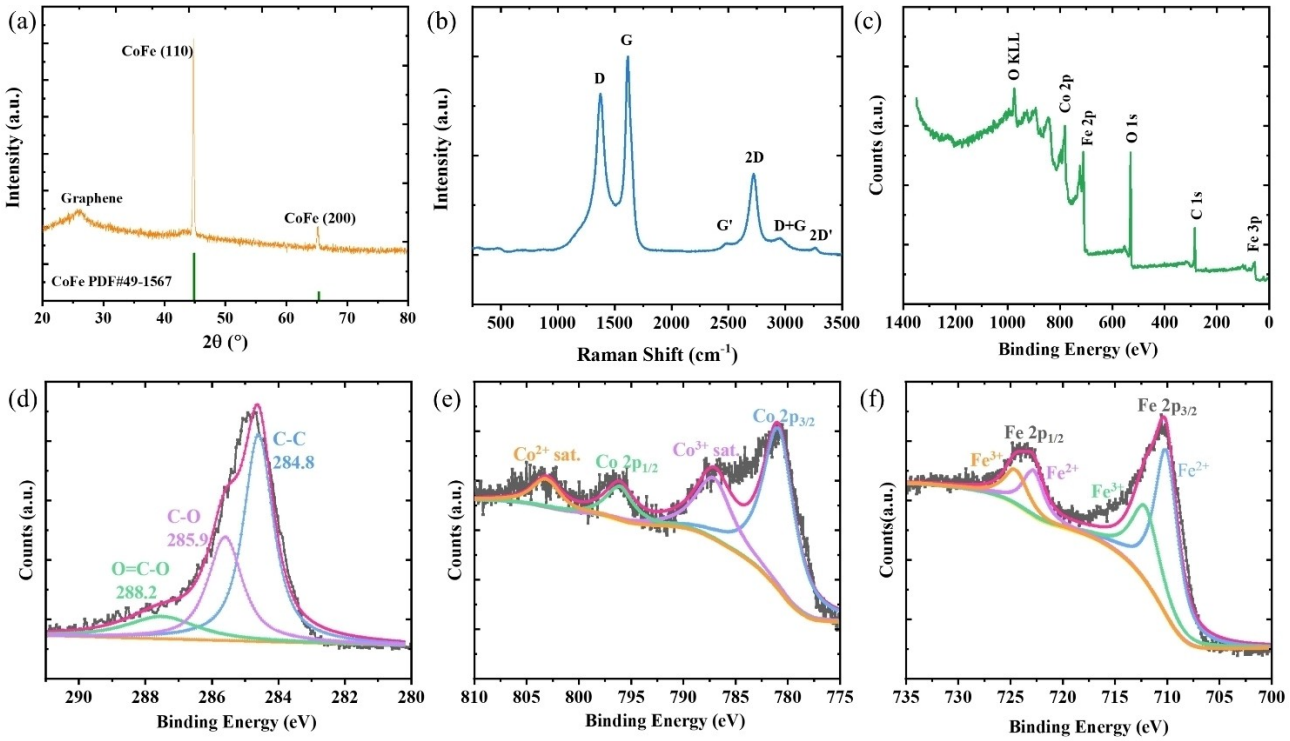

Figure 2. The crystal structure, element composition and bonding state of the $CoFe_2$ alloy/FLGs nanocomposite. (a) XRD pattern; (b) Raman spectrum; (c) XPS full spectrum; (d) High-resolution C 1s spectrum; (e) High-resolution Co 2p spectrum; (f) High-resolution Fe 2p spectrum.

0.353 nm, consistent with the theoretical plane spacing of graphene (0.350 nm). The difference between the number of graphene layers and the number of peaks is approximately 5. The lattice spacing of $CoFe_2$ particles in S2 was determined to be 0.203 nm, corresponding to the $CoFe_2$ (110) plane. The elemental mapping in Figure 1f depicts the distribution of nanoparticles containing Fe and Co atoms within the C (or graphene) layer.

The crystal structure of the $CoFe_2$ alloy was analyzed using XRD, and two distinctive peaks of the $CoFe_2$ alloy are presented in Figure 2a. The crystallinity size of the $CoFe_2$ alloy was approximately 25 nm, as determined by the Scherrer equation. A weak diffraction peak at 25° was attributed to graphene. The low intensity of the graphene diffraction peak can be attributed to the presence of only a few layers of graphene. The crystallinity of the graphene was evaluated using Raman spectroscopy, which reveals six characteristic peaks in Figure 2b. The prominent G peak signifies the high crystallinity of the graphene, while the broadened shape of the 2D peak indicates the presence of few graphene layers.[29] Figure 2c illustrates the full XPS spectra of the $CoFe_2$ alloy/FLGs composite, showcasing the presence of four elements: Co, Fe, O, and C, without any other elements. The high-resolution C 1s spectra in Figure 2d are decomposed into three distinct peaks at 284.8 eV (C–C), 285.9 eV (C–O), and 288.2 eV (O=C–O). The high-resolution Fe 2p and Co 2p spectra depicted in Figure 2e and 2f predominantly consist of (Fe^{3+}, Fe^{2+}) and (Co^{3+}, Co^{2+}) species, aligning with the typical Fe and Co spectra.

The magnetic properties of the $CoFe_2$ alloy/FLGs nanocomposite were investigated under applied magnetic fields ranging from −5000 Oe to 5000 Oe, as depicted in Figure 3. The $CoFe_2$ alloy/FLGs composite exhibited typical soft magnetic behavior, with values of saturation magnetization (*Ms*) and coercivity (*Hc*) measured at 351.0 emu/g and 106.5 Oe, respectively. These results indicate that the composite possesses higher magnetism compared to other metals and metallic oxides.[24,26,27] The inset of Figure 3 illustrates the magnetic response of the $CoFe_2$ alloy/FLGs nanocomposites to an

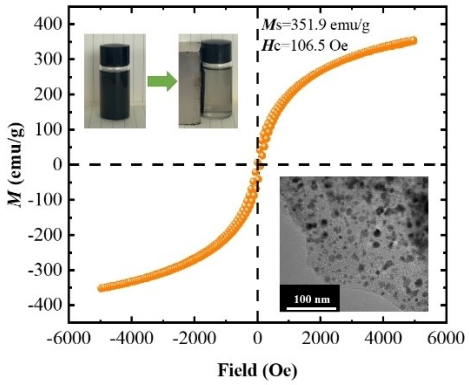

Figure 3. Hysteresis loop of $CoFe_2$ alloy/FLGs nanohybrid, the digital photos in the top left corner depict the magnetic response of the $CoFe_2$ alloy/FLGs nanohybrid to an external magnetic field. The TEM image in the bottom right corner illustrates the morphology of the nanohybrid after exposure to a strong magnetic field.

external magnetic field. Upon placing a magnet around the container, the $CoFe_2$ alloy/FLGs composite in ethanol solvent rapidly separated from the solution, indicating a strong binding between the graphene and $CoFe_2$ alloy particles. Moreover, the separated solution appeared clear, enabling convenient recovery of the $CoFe_2$ alloy/FLGs composite. The morphology of the materials was analyzed using TEM, and the results are presented in the insert of Figure 3. A comparison of the morphology before and after exposure to a strong magnetic field reveals nearly identical characteristics, indicating a robust binding between the graphene and $CoFe_2$ alloy particles. This observation further supports the notion of a strong interaction between the two components.

The oxygen reduction catalytic activity of the $CoFe_2$ alloy/FLGs nanocomposite was evaluated using cyclic voltammetry (CV) in a 0.1 mol/L KOH solution saturated with N_2 and O_2. The CV curves are presented in Figure 4a, where the reduction peak is only observed in the presence of O_2. The oxygen reduction peak potential (Epeak) of the $CoFe_2$ alloy/FLGs nanocomposite is measured at 0.78 V, indicating its excellent ORR catalytic activity. Additionally, a peak observed at 0.5 V during the anodic scan can be attributed to the oxidation of metallic Co and Fe, leading to the formation of Co (II) and Fe (III)/Fe (II). In the cathodic scan, two peaks at −0.1 V and 0.1 V correspond to the reduction of Co (II) and Fe (III)/Fe (II) back to metallic Co and Fe.[30]

Figure 4b depicts the linear sweep voltammetry (LSV) of the $CoFe_2$ alloy/FLGs catalyst obtained at different rotational speeds (250 to 3000 r/min) with a scan rate of 10 mV/s in a potential window of −0.2 to +1.2 V. The corresponding Koutecky-Levich (K-L) plots and electron transfer numbers at different electrode potentials are also displayed. It can be observed that the catalyst's limiting current increases with an increase in rotational speed, suggesting that the oxygen reduction process is influenced by the oxygen diffusion rate. Figure 4c gives the LSV curves of the $CoFe_2$ alloy/FLGs nanocomposite and commercial Pt/C at a rotation rate of 1600 r/min. The $CoFe_2$ alloy/FLGs nanocomposite exhibits a higher onset potential (0.901 V) compared to other reported catalysts, such as FLGs, $CoFe_2O_4$/N-rGO, $NiFe_2O_4$/N-Gr nanohybrid, $CoFe_{2-x}Zr_xO_4$/r-GO, and $CoFe_2O_4$/rGO, as shown in Table 1.[31–37] This onset potential is similar to that of the commercial Pt/C electrocatalyst (0.905 V). Additionally, the K-L curves of the $CoFe_2$ alloy/FLGs nanocomposite (insets of Figure 4b) demonstrate a good linear relationship between J^{-1} and $\omega^{-1/2}$, indicating that the oxygen reduction reaction catalyzed by the nanocomposite follows a first-order kinetic reaction polarization curve.[38] Moreover, the electron transfer number (n) for the ORR was determined using the K-L equation based on the K-L curve. In the voltage range of 0.1–0.4 V, the number of electrons transferred at 0.1 V, 0.2 V, 0.3 V, and 0.4 V is measured to be 4.10, 4.00, 3.90, and 3.70, respectively, indicating that the $CoFe_2$ alloy/FLGs nanocomposite follows a four-electron pathway.

Furthermore, the rotating ring disk electrode (RRDE) test provides additional insights into the oxygen reduction reaction mechanism and intermediates. During the oxygen reduction reaction, the intermediate peroxide produced at the disk electrode diffuses onto the platinum ring located at the periphery of the disk as the electrode rotates. By applying a higher voltage (0.5 V) to the platinum ring than to the disk, the

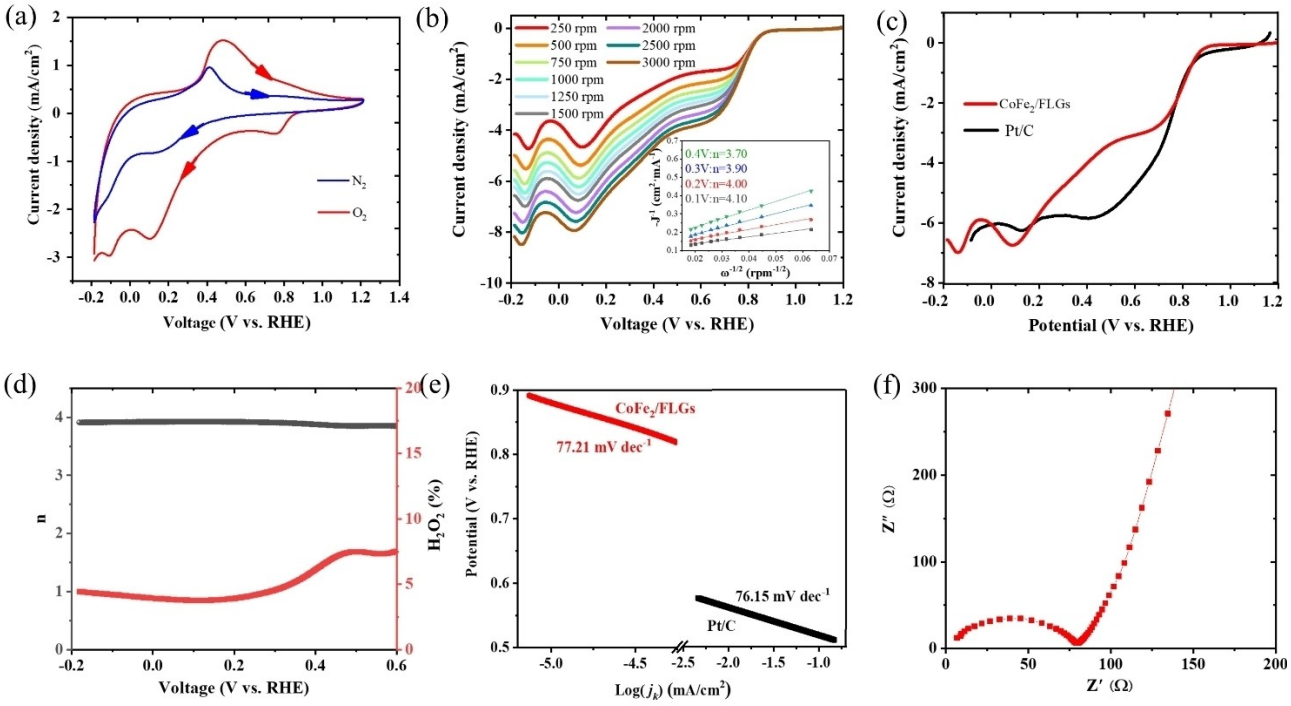

Figure 4. ORR performance of the $CoFe_2$/FLGs material. (a) CV curves in N_2-saturated and O_2-saturated solution; (b) LSV in O_2-saturated solution recorded at rotation rates of 250–3000 rpm, the insets are K-L plots and electron transfer number; (c) LSV curves at 1600 rpm of $CoFe_2$/FLGs and Pt/C; (d) Electron transfer number n vs potential and H_2O_2 yield versus potential; (e) Tafel plot; (f) EIS plot.

Table 1. Comparing the ORR performance of various samples in the literature works.

Catalyst	Loading (mg/cm^2)	Sweep rate (mV/s)	Electrolyte	Onset potential (V)	Tafel slope (mV/dec)	Rct (Ω)	Ref.
$CoFe_2$/FLGs	0.41	10	0.1 M KOH	0.901	77.21	72	This work
Fe/Fe_3C/FLGs	0.32	10	0.1 M NaOH	0.96	78.46	73	[31]
Fe–N/rGO	0.318	10	0.1 M KOH	0.885	80	–	[32]
$NiFe_2O_4$/N-G	0.64	10	0.1 M KOH	0.87	91	–	[33]
NC@CoFe-$CoFe_2O_4$	0.2	5	0.1 M KOH	1.0	74.5	–	[34]
$CoFe_2O_4$/N-rGO	1.2	50	0.1 M KOH	0.872	–	44	[35]
$CoFe_2$-xZr_xO_4/ r-GO	2	10	0.1 M KOH	0.84	–	–	[36]
$CoFe_2O_4$/rGO	0.401	10	0.1 M KOH	0.86	68	200	[37]

peroxide reaching the ring undergoes rapid oxidation, resulting in a ring current. The calculation of H_2O_2% and electron transfer number (n) is determined using the following equations:[39,40]

$$H_2O_2(\%) = 200^* \frac{\frac{I_r}{N}}{\frac{I_r}{N} + I_d} \quad (1)$$

$$n = 4^* \frac{I_d}{\frac{I_r}{N} + I_d} \quad (2)$$

where I_d and I_r represent the disc current and ring current respectively, and the collection coefficient of the electrode is denoted by N = 0.38. Figure 4d displays the variation of the number of electron transfer (n) and the H_2O_2 generation on $CoFe_2$ alloy/FLGs. As depicted in Figure 4d, the H_2O_2 yield of $CoFe_2$ alloy/FLGs is below 7.5% in the potential range of −0.2~0.6 V, and the n value of $CoFe_2$ alloy/FLGs is 3.85–3.92, which is consistent with the K-L analysis, indicating excellent 4-electron reaction selectivity. This selectivity is beneficial for improving the energy conversion efficiency and fuel cell lifetime.

The ORR kinetic characteristics of the catalyst were assessed using the Tafel curve (Figure 4e), and the Tafel slopes of the linear polarization region were calculated for the $CoFe_2$ alloy/FLGs nanocomposite at a scan rate of 10 mV/s. A smaller Tafel slope indicates faster reaction kinetics and better ORR electrocatalytic activity. As shown in Figure 4e, the Tafel slope of the $CoFe_2$ alloy/FLGs nanocomposite is measured to be 77.21 mV/dec, which is smaller than that of the reported Fe-N/rGO,[32] and $NiFe_2O_4$/N-G.[33] It is also comparable to the Tafel slope of the NC@CoFe-$CoFe_2O_4$,[34] $CoFe_2O_4$/rGO,[37] and commercially available Pt/C electrocatalyst (~76.15 mV/dec). This Tafel slope of the $CoFe_2$ alloy/FLGs nanocomposite is also similar to our previous work on Fe/Fe_3C/FLGs (78.46 mV/dec). Furthermore, the electrochemical impedance spectroscopy (EIS) of the $CoFe_2$ alloy/FLGs nanocomposite was measured, and the Nyquist plots are presented in Figure 4f. Clearly, the $CoFe_2$ alloy/FLGs nanocomposite exhibits lower charge-transfer resistance (Rct) (~72 Ω) compared to the reported FLGs (~290 Ω).[31]

Besides activity, stability is a crucial parameter for high-performance electrocatalysts. The stability of the $CoFe_2$ alloy/FLGs nanocomposite as an electrocatalyst was assessed under a voltage sweep rate of 10 mV/s in an oxygen-saturated 0.1 M KOH solution. Figure 5a displays the cyclic voltammetry (CV) curves of the $CoFe_2$ alloy/FLGs nanocomposite before and after 1000 cycles. It is observed that the oxygen reduction peak experiences minimal shifting, and the area of the loop retains approximately 85% of its initial value. These results indicate the exceptional stability of the $CoFe_2$ alloy/FLGs materials. The methanol resistance ability of the $CoFe_2$ alloy/FLGs nanocomposite during ORR was evaluated and compared to that of the commercial Pt/C catalyst. After the current stabilized, methanol was injected into the solution at 1000 s. As depicted in Figure 5b, the relative current (I/I_0) of the commercial Pt/C catalyst drops significantly, while that of the $CoFe_2$ alloy/FLGs nanocomposite undergoes no significant change. This demonstrates that the $CoFe_2$ alloy/FLGs nanocomposite exhibits superior and stable electrochemical catalytic activity compared to the commercial Pt/C catalyst for methanol oxidation.

Prior to this work, we fabricated a Fe/Fe_3C/FLGs composite using ferric nitrate and glucose as precursors, which exhibited high-performance ORR electrocatalytic activity. In this study, the obtained $CoFe_2$ alloy/FLGs nanocomposite not only demonstrates excellent ORR performance but also shows high recyclability due to the high magnetism of the $CoFe_2$ alloy particles.

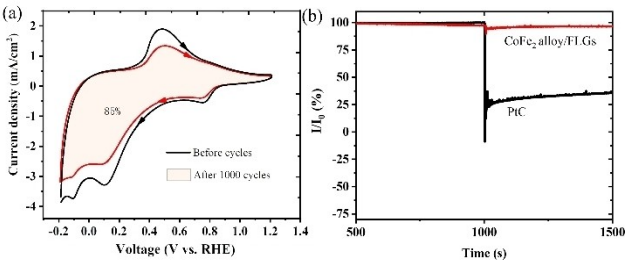

Figure 5. (a) CV curves of $CoFe_2$/FLGs material before and after 1000 cycles; (b) Resistance to methanol poisoning for $CoFe_2$/FLGs and Pt/C.

Conclusions

The $CoFe_2$/FLGs nanocomposite was successfully fabricated and exhibited remarkable ORR catalytic activity and recyclability. Various characterizations confirmed the uniform distribution of nanosized $CoFe_2$ particles within the FLGs. Electrochemical analyses demonstrated the high catalytic activity of the $CoFe_2$/FLGs nanocomposite for oxygen reduction, as well as low H_2O_2 yield and superior stability compared to commercial Pt/C. These findings suggest that the obtained $CoFe_2$/FLGs nanocomposite is an efficient and recyclable non-precious metal catalyst, holding great potential for fuel cell catalyst research.

Competing Financial Interests

The authors declare that they have no known competing financial interests or personal relationships that could have appeared to influence the work reported in this paper.

Acknowledgements

This work is funded by the Fundamental Research Funds for the Provincial Universities of Zhejiang (GK239909299001-402), National Natural Science Foundation of China (Grant No. 51702075).

Conflict of Interests

The authors declare no conflict of interest.

Data Availability Statement

The data that support the findings of this study are available from the corresponding author upon reasonable request.

Keywords: alloy · catalyst · electrochemistry · graphene · ORR

[1] M. K. Debe, *Nature* **2012**, *486*, 43–51.
[2] H. Singh, S. Zhuang, B. Ingis, B. B. Nunna, E. S. Lee, *Carbon* **2019**, *151*, 160–174.
[3] N. Jung, D. Y. Chung, J. Ryu, S. J. Yoo, Y. E. Sung, *Nano Today* **2014**, *9*, 433–456.
[4] A. Kulkarni, S. Siahrostami, A. Patel, J. K. Nørskov, *Chem. Res.* **2018**, *118*, 2302–2312.
[5] J. Lee, B. Jeong, J. D. Ocon, *Curr. Appl. Phys.* **2013**, *13*, 309–321.
[6] F. J. Yin, Y. Liu, S. Wang, C. Wang, H. Liu, *Electrochim. Acta* **2019**, *313*, 378–388.
[7] G. Wu, P. Zelenay, *Chem. Res.* **2013**, *46*, 1878–1889.
[8] R. Othman, A. L. Dicks, Z. Zhu, *Int. J. Hydrogen Energy* **2012**, *37*, 357–372.
[9] F. Y. Cheng, J. Shen, B. Peng, *Nat. Chem.* **2011**, *3*, 79–84.
[10] A. Brouzgou, S. Q. Song, P. Tsiakaras, *Appl. Catal. B* **2012**, *127*, 371–388.
[11] X. F. Ren, Q. Y. Lv, L. F. Liu, B. H. Liu, Y. R. Wang, A. M. Liu, G. Wu, *Sustain. Energy Fuels* **2020**, *4*, 15–30.
[12] W. He, H. J. Jiang, Y. Zhou, S. D. Yang, X. Z. Xue, Z. Q. Zou, X. G. Zhang, D. L. Akins, H. J. Yang, *Carbon* **2012**, *50*, 265–274.
[13] Y. H. Bing, H. S. Liu, L. Zhang, D. Ghosh, J. J. Zhang, *Chem. Soc. Rev.* **2010**, *39*, 2184–2202.
[14] D. Banham, S. Ye, *ACS Energy Lett.* **2017**, *2*, 629–638.
[15] M. H. Shao, Q. W. Chang, J. P. Dodelet, R. Chenitz, *Chem. Res.* **2016**, *116*, 3594–3657.
[16] Y. Nie, L. Li, Z. D. Wei, *Chem. Soc. Rev.* **2015**, *46*, 2168–2201.
[17] X. Chen, S. J. Chen, J. Y. Wang, *Appl. Surf. Sci.* **2016**, *379*, 291–295.
[18] Y. Y. Wang, S. Liu, R. P. Li, Y. P. Huang, C. C. Chen, *J. Environ. Sci-china.* **2016**, *43*, 54–60.
[19] Q. Tang, Z. Zhou, Z. F. Chen, *WIREs Comput. Mol. Sci.* **2015**, *5*, 360–379.
[20] X. W. Wang, G. Z. Sun, P. Routh, D. H. Kim, W. Huang, *Chem. Soc. Rev.* **2014**, *43*, 7067–7098.
[21] M. L. Xiao, J. B. Zhou, C. P. Liu, J. J. Ge, W. Xing, *J. Electrochem.* **2016**, *22*, 101.
[22] H. L. Fei, J. C. Dong, Y. X. Feng, C. S. Allen, C. Z. Wan, B. Volosskiy, M. F. Li, Z. P. Zhao, Y. L. Wang, H. T. Sun, P. F. An, W. X. Chen, Z. Y. Guo, C. Lee, D. L. Chen, I. Shakir, M. J. Liu, T. D. Hu, Y. D. Li, A. I. Kirkland, X. F. Duan, Y. Huang, *Nat. Catal.* **2018**, *1*, 63–72.
[23] S. Bukola, B. Merzougui, A. Akinpelu, M. Zeama, *Electrochim. Acta* **2016**, *190*, 1113–1123.
[24] J. Wang, G. X. Wang, S. Miao, X. L. Jiang, J. Y. Li, X. H. Bao, *Carbon* **2014**, *75*, 381–389.
[25] R. X. Wang, P. Y. Zhang, Y. C. Wang, Y. S. Wang, K. Zaghib, Z. Y. Zhou, *Prog. Nat. Sci-Mater.* **2020**, *30*, 855–860.
[26] S. J. Guo, S. Zhang, L. H. Wu, S. H. Sun, *Angew. Chem. Int. Ed.* **2012**, *51*, 11770–11773.
[27] Q. Q. Feng, Z. F. Chen, K. Zhou, M. L. Sun, X. R. Ji, H. Zheng, Y. Zhang, *ChemistrySelect* **2021**, *6*, 8177–8181.
[28] L. N. Fan, W. Chen, K. Zhou, H. Zheng, P. Zheng, L. Zheng, Y. Zhang, *ACS Appl. Electron. Mater.* **2023**, *5*, 123–131.
[29] G. E. Scuseria, *Science* **1996**, *271*, 942–945.
[30] W. R. P. Barros, Q. L. Wei, G. X. Zhang, S. H. Sun, M. R. V. Lanza, A. C. Tavares, *Electrochim. Acta* **2015**, *162*, 263–270.
[31] M. L. Sun, F. Y. Yuan, R. Q. Li, S. J. Dong, Y. Zhao, W. X. Zhong, C. Shen, J. P. Wu, H. Zheng, *ACS Omega* **2022**, *7*, 25458–25465.
[32] X. Deng, M. L. Xiao, R. Yang, F. Guo, H. Q. Chen, Y. Hu, Y. Li, C. C. Zhu, Y. P. Deng, Z. Jiang, Z. Xu, C. Gao, Q. G. He, J. J. Ge, Y. Hou, X. W. Zhang, Z. W. Chen, *J. Electrochem. Soc.* **2018**, *165*, F401.
[33] M. Kiani, J. Zhang, J. L. Fan, H. W. Yang, G. Wang, J. W. Chen, R. L. Wang, *Mater. Express* **2017**, *7*, 261–272.
[34] M. Qian, X. Cheng, T. Sun, J. Tian, T. T. Isimjan, Z. Shi, X. Yang, *J. Alloys Compd.* **2019**, *819*, 153015.
[35] V. Kashyap, S. K. Singh, S. Kurungot, *ACS Appl. Mater. Interfaces* **2016**, *8*, 20730.
[36] V. Kashyap, S. Kurungot, *ACS Catal.* **2018**, *8*, 3715–3726.
[37] W. N. Yan, X. C. Cao, K. Ke, J. H. Tian, C. Jin, R. Z. Yang, *RSC Adv.* **2016**, *6*, 307–313.
[38] R. Nandan, A. Gautam, S. Tripathi, K. K. Nanda, *J. Mater. Chem. A* **2018**, *6*, 8537–8548.
[39] X. L. Wang, J. Du, Q. H. Zhang, L. Gu, L. Cao, H. Liang, *Carbon* **2020**, *157*, 614–621.
[40] C. Wang, Z. F. Li, L. K. Wang, X. L. Niu, S. W. Wang, *ACS Sustainable Chem. Eng.* **2019**, *7*, 13873–13885.

Manuscript received: May 15, 2023